physchem

MDPI

Article

Enhanced Cadmium Removal by Raw Argan Shell Adsorbent: Experimental and Theoretical Investigations for Ecological Applications

Fatima-Zahra Abahdou [1], Maria Benbouzid [1], Khalid Bouiti [2], Hamid Nasrellah [3], Meryem Bensemlali [4], Najoua Labjar [2] and Souad El Hajjaji [1,*]

[1] Laboratory of Spectroscopy, Molecular, Modeling, Materials, Nanomaterials, Water and Environment, (LS3MNWE), Department of Chemistry, Faculty of Sciences, Mohammed V University in Rabat, Av. Ibn Battouta, B.P. 1014, Rabat 10000, Morocco; fatimazahra_abahdou@um5.ac.ma (F.-Z.A.); mariabenbouzid@hotmail.fr (M.B.)

[2] Laboratory of Spectroscopy, Molecular, Modeling, Materials, Nanomaterials, Water and Environment, (LS3MNWE), ENSAM-Rabat, Mohammed V University in Rabat, Av. Ibn Battouta, B.P. 1014, Rabat 10000, Morocco; khalid.bouiti.khb@gmail.com (K.B.); najoua.labjar@ensam.um5.ac.ma (N.L.)

[3] Higher School of Education and Training, Chouaib Doukkali University, El Jadida 24000, Morocco; nasrellah.h@ucd.ac.ma

[4] Higher School of Education and Training, Mohammed I University, Oujda 60000, Morocco; bensemlali.m@ucd.ac.ma

* Correspondence: s.elhajjaji@um5r.ac.ma

Abstract: The removal of cadmium ions (Cd^{2+}) using raw argan shells (ArS) was optimized through experimental and theoretical studies. Adsorption experiments revealed optimal conditions at an adsorbent dose of 3.5 g, an initial Cd^{2+} concentration of 20 $mg{\cdot}L^{-1}$, and a pH of 8, achieving a maximum sorption capacity of 3.92 $mg{\cdot}g^{-1}$. The kinetic analysis showed that the adsorption followed a pseudo-second-order model ($R^2 = 0.98$), and the Langmuir isotherm model predicted a maximum adsorption capacity of 4 $mg{\cdot}g^{-1}$. Thermodynamic analysis indicated an endothermic adsorption process, with ΔG° shifting from positive to negative as temperature increased, confirming that adsorption is favored at higher temperatures. Desorption studies demonstrated that HCl was the most effective eluting agent, achieving a desorption efficiency of 90.02%, followed by HNO_3 (76.65%) and CH_3COOH (71.59%). The varying desorption efficiencies were attributed to differences in acid strength and ionic interactions with Cd^{2+}. This study demonstrates the potential of raw argan shells as an efficient, reusable, and sustainable biosorbent for cadmium removal, offering a promising solution for water treatment and environmental remediation.

Keywords: biosorption; argan nut shell; cadmium (II); kinetic; experimental design

check for updates

Academic Editor: Francesco Mallamace

Received: 15 January 2025
Revised: 15 February 2025
Accepted: 19 February 2025
Published: 19 March 2025

Citation: Abahdou, F.-Z.; Benbouzid, M.; Bouiti, K.; Nasrellah, H.; Bensemlali, M.; Labjar, N.; El Hajjaji, S. Enhanced Cadmium Removal by Raw Argan Shell Adsorbent: Experimental and Theoretical Investigations for Ecological Applications. *Physchem* **2025**, *5*, 13. https://doi.org/10.3390/physchem5010013

Copyright: © 2025 by the authors. Licensee MDPI, Basel, Switzerland. This article is an open access article distributed under the terms and conditions of the Creative Commons Attribution (CC BY) license (https://creativecommons.org/licenses/by/4.0/).

1. Introduction

Heavy metals, including both transition and post-transition elements like lead, cadmium, thallium, and antimony, are commonly found in industrial environments and are significant environmental pollutants due to their hazardous nature [1]. Due to the growth of the mining sector and industrial activities, the discharge of heavy metals into the environment has increased [2]. These metal cations are commonly found in effluents from mining drainage, dye waste, paint and ink manufacturing, electroplating and porcelain polishing, and battery production. High concentrations of metal ions negatively affect water quality, aquatic life, terrestrial flora and fauna, and human health [3]. Heavy metal ions do not biodegrade like organic contaminants do; they cannot be broken down into harmless

by-products, leading to bioaccumulation in living organisms and eventual transmission across the food chain to humans [4]. Among these heavy metals, cadmium stands out due to its prevalence in various industrial processes and its particularly harmful impact on ecosystems and public health [5]. Indeed, the World Health Organization (WHO) categorizes cadmium as a highly toxic substance [6], and it is released through multiple industrial procedures such as the fabrication of electronic components and batteries. Additionally, cadmium pollution originates from agricultural sources, as cadmium is often present in phosphate fertilizers due to its occurrence in phosphate rock, the primary raw material used to produce these fertilizers [7]. When phosphate rock is processed to extract phosphoric acid (the key component of phosphate fertilizers), cadmium, which can be found in concentrations ranging from 10 to 80 g per ton in phosphate minerals, may also be released and remain in the final product [6]. Despite being a relatively minor constituent of phosphate rock, the accumulation of cadmium in fertilizers poses significant environmental and health risks. When such fertilizers are used on farmland, cadmium has the potential to infiltrate soil and water systems [8]. Several studies have shown that cadmium accumulates in soils and seeps into groundwater and surface waters, exhibiting bioaccumulative properties. Eutrophication is one of the issues associated with the use of phosphate fertilizers, significantly impacting the environment [9]. However, cadmium pollution in aquatic ecosystems continues to be a worldwide problem. Research has established a direct link between cadmium exposure and bone and kidney issues, as it disrupts filtration mechanisms and can potentially lead to liver cancer [6]. Even at low quantities, cadmium can be harmful to human health, hence it is imperative that contaminated water sources be treated to ensure environmental and public health. Given the negative effects associated with this situation, international regulatory bodies have urged the implementation of strict regulations limiting the discharge of heavy metals into sewers and receiving waterways [10]. Therefore, it is crucial to develop techniques that are both cost-efficient and environmentally friendly to remove metallic cations from wastewater [11]. Although challenging, the removal of these metal cations can be achieved through various traditional treatment methods, including ion exchange, chemical precipitation, coagulation–flocculation, and flotation [12]. These techniques have several disadvantages, namely expensive implementation, insufficient selectivity, and only partial elimination of metal ions, particularly when the concentration is less than 50 $mg \cdot L^{-1}$ [9]. Consequently, it is essential to create a new affordable technique to minimize damage. For this purpose, biosorption presents a potential method. Several research studies have been released regarding the possibility of biosorbents to remove cadmium ions from an aqueous medium, such as pine bark, walnut shells, cashew activated carbon, raw walnut shells, coffee beans, rice husk ash, activated carbon obtained from the husk of rice, and *Pachira aquatica* Aubl. fruit peels [13–20]. This process is technically an effective method for eliminating inorganic and organic contaminants in an aqueous solution. Recent research has also explored the use of mesoporous silica derivatives for the selective recovery of cadmium, cobalt, and nickel from Ni-Cd batteries [21], highlighting the importance of porous materials in heavy metal adsorption. However, since the argan tree is a naturally abundant and unique resource in Morocco, argan shells are readily accessible and affordable [22]. Utilizing this agricultural waste not only meets a local need by adding value to an unexploited by-product but also lowers the total cost of the adsorption process. Furthermore, argan shells possess physicochemical properties favorable for heavy metal adsorption. Their porous structure and chemical composition allow effective interaction with metal ions, maximizing adsorption capacity [23]. These characteristics make argan shells an excellent candidate compared to other biomaterials, contributing to an eco-friendly and sustainable solution for decontaminating polluted water sources.

To our knowledge, this is the first study to specifically evaluate the adsorption potential of raw argan nut shells for cadmium removal from aqueous solutions. This study highlights the untapped potential of a local, natural resource from Morocco, contributing to the development of an eco-friendly and cost-effective biosorbent for heavy metal remediation. Consequently, the aim of this study is to remove cadmium cations (Cd^{2+}) from contaminated water through biosorption using natural adsorbents, specifically raw argan nut shells, which are considered an untapped plant waste with significant potential. This experiment was conducted in a controlled cadmium solution, rather than actual wastewater, to precisely evaluate the adsorption capacity of argan powder for cadmium.

2. Materials and Methods

2.1. Natural Adsorbent: Preparation of Argan Nut Shell Powder (ArS)

Argan shells, harvested near Aoulouz, were first broken into small fragments using a Retsch RM 200 mortar grinder in their natural state (referred to as ArS). The primary purpose of mechanical grinding was to reduce crystallinity levels [24]. The resulting powder was then sieved to achieve particle sizes between 125 and 63 µm in diameter. After sieving, the powder was cleaned with hot bi-distilled water to effectively remove all contaminants, followed by a drying phase.

2.2. Adsorbate: Synthetic Solution Preparation

To prepare the cadmium stock solution, 10 mg of cadmium chloride ($CdCl_2$) was dis-solved in 100 mL of ultrapure water sourced from a Millipore Milli-Q system, where the resistivity is more than 18 MΩ·cm at ambient temperature. The $CdCl_2$, sourced from Sigma Aldrich, possesses a molecular weight of 183.32 $g{\cdot}mol^{-1}$, a water solubility of 119.6 g/100 mL at ambient temperature, and a purity of 99.99%. From this stock solution, three working solutions were prepared with Cd^{2+} concentrations of 5 $mg{\cdot}L^{-1}$, 12.5 $mg{\cdot}L^{-1}$, and 20 $mg{\cdot}L^{-1}$ to evaluate the adsorption of cadmium by argan shell powder. pH adjustments were per-formed directly in the working solutions using high-quality reagents, NaOH (99.0%) and HCl (37%), obtained from Merck & Co. (Darmstadt, Germany).

2.3. Characterization

2.3.1. Scanning Electron Microscopy (SEM-EDX)

A SEM-EDX study was performed to examine the surface elemental composition and morphology of ArS. The measurements were performed utilizing a JEOL JSM-IT100 scanning electron microscope, operated at an acceleration voltage of 20 kV.

2.3.2. FTIR Analysis

Infrared transmission spectra were recorded using a PerkinElmer RX-1 spectrometer. A sample pellet with 1 wt% concentration was dispersed in KBr for analysis. The infrared spectrum was measured between 4000 and 500 cm^{-1}, with a 4 cm^{-1} spectral resolution.

2.3.3. pH Zero Charge Point: pH_{zpc}

pH_{zpc} provides valuable insight into the electrostatic forces involved in adsorption [25]. In this analysis, 0.15 g of ArS was suspended in 50 mL of NaCl solution at a concentration of 0.01 M, with the initial pH adjusted from 2 to 12. Suspensions were agitated for 48 h and then filtered, after which the final pH (pH_f) was measured. The variation in pH ($\Delta pH = pH_f - pH_i$) was graphed relative to the starting pH (pH_i), and the pH_{zpc} was determined at the point where the curve crosses the axis of zero.

The pH_{zpc} provides useful information on the electronic and chemical characteristics of the surface groups [26].

2.3.4. Boehm Titration

The functional groups present on the surface of ArS were analyzed using the method of Boehm, which allows for a global determination of basic functions while measuring acidic functions individually. In this method, 0.15 g of ArS was added to 50 mL of aqueous solutions of NaOH, Na_2CO_3, and $NaHCO_3$, as well as a 0.01 M HCl solution. NaOH neutralizes all lactonic, phenolic, and carboxylic functions; sodium carbonate neutralizes lactonic and carboxylic functions; and sodium bicarbonate neutralizes only carboxylic functions on the surface of the material. Each solution was stirred for 24 h to ensure that the majority of the functional groups reacted, after which the solutions were filtered. The final step involved titrating a 10 mL sample from each filtrate using alkaline solutions against 0.01 M HCl and acidic solutions against 0.01 M NaOH [27].

2.3.5. Specific Area

The knowledge of the mass area of a sample, referred to as the specific surface area, is of great importance in physicochemical studies, particularly in the adsorption field. The specific surface area is essential for characterizing finely divided solids and porous materials, as it is directly related to the reactivity of the solid. To determine the surface area of ArS, the methylene blue technique was utilized. In this experiment, 0.1 g of ArS was combined with 50 mL of prepared mixture at various concentrations, agitated for 2 h, and then filtered. The filtrate was subsequently analyzed. The Langmuir model was applied, using the equation below, to evaluate the available surface area [28]:

$$S_a = (Q_m \times N_A \times S)/M \quad (1)$$

where S_a represents the surface area ($m^2 \cdot g^{-1}$); Q_m denotes the highest adsorption capacity, expressed in $mg \cdot g^{-1}$; N_A represents the Avogadro number which is 6.023×10^{23} mol^{-1}; S refers to the area occupied by a single methylene blue molecule, which is equal to 119 $Å^2$; and M represents the molar mass of hydrated methylene blue which is 319.86 $g \cdot mol^{-1}$.

2.3.6. Inductively Coupled Plasma Mass Spectrometry (ICP-MS)

ICP-MS was utilized to perform all trace element analyses in this study, employing a Thermo Scientific X-SERIES 2 instrument (Waltham, MA, USA). This highly sensitive and precise technique allows for the detection of trace elements at low concentrations, making it particularly valuable for analyzing heavy metals, such as cadmium, in environmental samples.

2.4. Response Surface Methodology (RSM): Batch Experiments

RSM is a powerful statistical tool used to optimize batch adsorption experiments by modeling how independent factors and response are related. It efficiently determines optimal conditions for adsorption systems, reducing the need for extensive experimentation [29]. In this study, analyses were conducted using RSM via JMP 17.2 software, which combines statistical and mathematical approaches [26]. This software enabled the evaluation of parameter influences on process efficiency and interaction effects through a predictive model [26]. The experimental design applied a second-degree polynomial function, utilizing the Box–Behnken optimization design with three factors: X_1 (initial concentration), X_2 (pH), and X_3 (adsorbent dose), with coded levels listed in Table 1.

Table 1. Selected trial levels applied to cadmium adsorption on ArS.

Variables	Code	−1	0	+1
$[Cd^{2+}]_i$ ($mg \cdot L^{-1}$)	X1	5	12.5	20
pH	X2	4	6	8
ArS dose ($g \cdot L^{-1}$)	X3	1	2.5	4

With $[Cd^{2+}]_i$ = Cd^{2+} initial concentration.

2.5. Batch Adsorption Process

Three input factors with three evenly distributed values, represented by −1, 0, and 1, were investigated during the batch adsorption studies, in the manner described in Table 1. The ideal adsorption conditions were determined by varying the Cd^{2+} concentration from 5 to 20 $mg \cdot L^{-1}$, the pH within the range of 4 to 8, and the ArS dose between 1 and 4 $g \cdot L^{-1}$ of 50 mL. The blend was agitated at 250 rpm under a temperature of 25 °C. Following the adsorption experiment, the ArS was isolated from the mixture using a 185 mm diameter Whatman Grade 595 filter paper. Residual Cd^{2+} concentrations in the liquid phase were analyzed using AES HORIBA ULTIMA EXPERT 2 (ICP-AES) (Loos, France). The adsorption capacity, expressed in milligrams of Cd^{2+} ions for every gram of ArS adsorbent, was determined utilizing the Formula (2) below Es-said [30]:

$$q_t = (C_0 - C_t) \cdot V/m \quad (2)$$

where C_0 and C_t represent the initial and final concentrations of heavy metal ions, respectively ($mg \cdot L^{-1}$), V is the volume of the entire solution (L), and m represents the mass of ArS adsorbent (g).

Various kinetic models, including pseudo-first-order and pseudo-second-order intraparticle diffusion, were employed to assess the kinetics of adsorption. Additionally, adsorption isotherm parameters were determined utilizing the Temkin, Dubinin–Radushkevich, Freundlich, and Langmuir models. Furthermore, the effect of temperature on the adsorption process was analyzed at 25 °C, 35 °C, 50 °C, and 65 °C, allowing us to calculate the associated thermodynamic factors.

3. Results and Discussion

3.1. Characterization

To characterize the ArS surface including its morphology and functional groups, SEM and FTIR techniques were employed, as adsorption is primarily a surface phenomenon.

3.1.1. SEM Analysis of Argan Nutshell Powder

The SEM image of argan nut shells in Figure 1 reveals key surface characteristics. The outer surface exhibits an irregular, heterogeneous texture with visible grooves and fissures contributing to a rough appearance. Small, uniformly distributed pores are also visible, suggesting the presence of intercellular cavities and micropores, which are advantageous for trapping and adsorbing metal cations. The ArS chemical composition was revealed using energy-dispersive X-ray spectroscopy (EDX), showing the material is primarily plant-based. Carbon is predominant at 53.09% of the weight, followed by oxygen at 45.98% and nitrogen in a smaller amount, with 0.94% by weight. This elemental profile reflects the organic nature of the material and highlights the potential of argan nut shells as an adsorbent due to the high carbon content, which is often associated with enhanced adsorption capabilities.

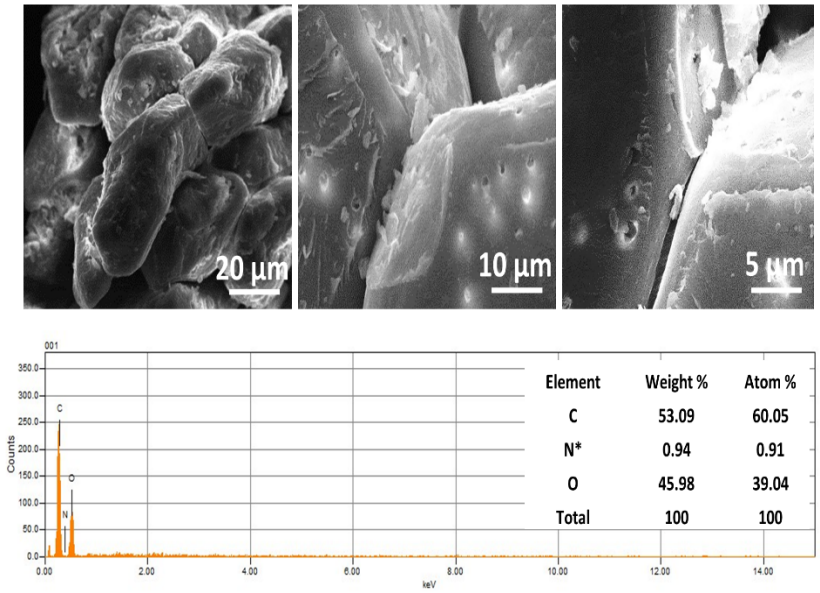

Figure 1. SEM images of Raw Argan shells and EDX analysis.

3.1.2. Fourier Transform Infrared Spectroscopy (FTIR)

The ArS FTIR spectrum, measured from 500 to 4000 cm^{-1} and shown in Figure 2, reveals characteristic absorbance bands corresponding to various functional groups. A prominent broad band at 3340.37 cm^{-1} suggests the detection of hydroxyl functional groups [31]. The presence of the OH band in the FTIR spectrum of raw argan shell, even without pretreatment, can be attributed to the intrinsic hydroxyl groups found in lignocellulosic components such as cellulose, hemicellulose, and lignin [32]. Additionally, the natural adsorption of atmospheric moisture and the formation of hydrogen bonds between hydroxyl groups contribute to the observed signal. Similar findings have been reported in other lignocellulosic biomass studies, confirming that untreated plant-based materials can exhibit OH stretching vibrations due to their inherent structure and surface properties.

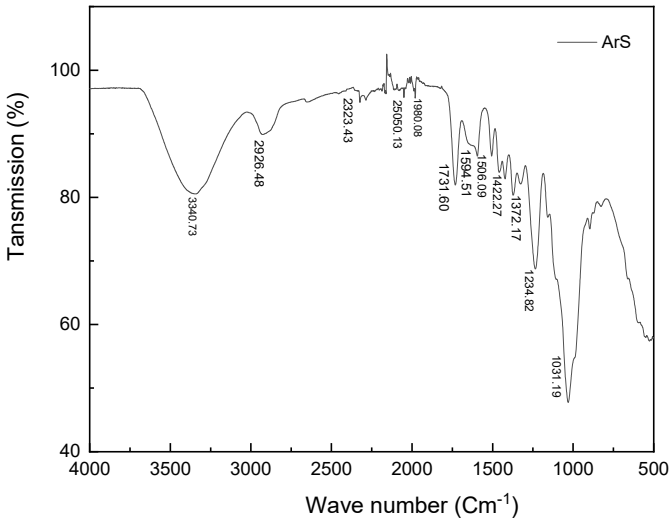

Figure 2. FTIR spectrum of ArS.

The peak detected around 1731.60 cm^{-1} is attributed to the stretching vibrations of C=O, likely from carboxylic acids or ester groups associated with lignin or hemicelluloses [31]. A peak at 1594.59 cm^{-1} indicates that the cellulose structure has absorbed water [33]. The band at 1422.27 cm^{-1} corresponds to CH_2 symmetric deformations in

cellulose [33]. The existence of CH and C=O groups in aromatic rings of polysaccharides is designated by the band at 1372.17 cm^{-1} [34]. Additionally, the absorbance band around 1234.82 cm^{-1} is linked to C=O stretching vibrations in acetyl groups within hemicellulose and lignin [31]. The band at 1031.13 cm^{-1} arises from C-O and O-H bond vibrations in the cellulosic structure [35], while a peak at 871.19 cm^{-1} corresponds to glycosidic bonds in polysaccharides. The last feature observed at 670.41 cm^{-1} is related to C-OH deformations in cellulose [36].

3.1.3. pH of Point Zero Charge: pH_{zpc}

Surface properties of the adsorbent play a crucial role in the relationship with the adsorbate during the sorption mechanism [37]. The pH_{zpc} represents the pH where the surface charge of the adsorbent becomes neutral, offering insights into reactive groups on the surface of the biosorbent and whether acidic or basic characteristics predominate. The pH_{zpc} of ArS was found experimentally at pH 3.6 (Figure 3). For pH levels exceeding the pH_{zpc}, the surface of ArS carries a negative charge, increasing the electrostatic attraction between metal cations and the surface, which increases cation adsorption [37]. Conversely, at pH values below pH_{zpc}, the biomass surface becomes positively charged, favoring interactions with anions. Additionally, decreased metal cation sorption can occur due to competitive sorption between H_3O^+ and Cd^{2+} ions. Therefore, pH_{zpc} plays a key role in controlling and enhancing the adsorption mechanism.

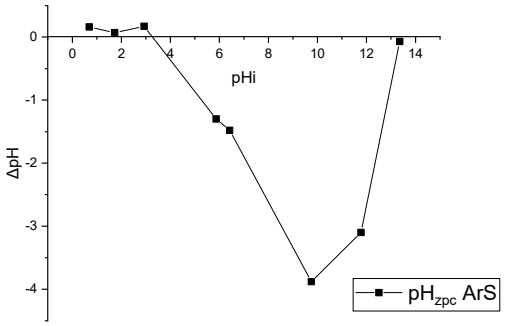

Figure 3. pH_{zpc} determination graph.

3.1.4. Boehm Titration

According to Boehm titration, the amount of functional groups that are acidic (0.133 $mmol \cdot g^{-1}$) on the adsorbent surface is greater than that of basic functional groups (0.092 mmol/g) (Table 2). This indicates that the majority of reactive sites within the adsorbent show acidity, suggesting a predominance of oxygenated surface-bound groups [38]. which are essential to the process of adsorption by enhancing the attraction of the adsorbent toward positively charged ions. The acidic nature of these functional groups contributes to a more negative surface charge once the pH level of the solution exceeds the ArS pH_{PZC} which is equal to 3.6. This negative surface charge increases the attraction of metal cations (Cd^{2+}) through electrostatic forces and the adsorbent, thereby improving the adsorption efficiency. In contrast, the lower quantity of basic functional groups suggests they play a less significant role in this context. Along with the functional groups, ArS surface area (31.99 $m^2 \cdot g^{-1}$) is an important factor that influences its adsorption capacity. A larger surface area generally enhances interaction with adsorbate molecules by offering additional adsorption active sites [39]. This relatively large surface area enables ArS to accommodate significant amounts of Cd^{2+}, which could improve adsorption process efficiency. Together, the large surface area and the acidic functional groups make ArS an effective adsorbent for targeting metal ions in aqueous solutions.

Table 2. Surface group quantification by Boehm titration of the surface area and pH_{zpc} value.

	Carboxylic Groups ($mmol \cdot g^{-1}$)	Phenolic Groups ($mmol \cdot g^{-1}$)	Lactonic Groups ($mmol \cdot g^{-1}$)	Total Acid ($mmol \cdot g^{-1}$)	Total Basic ($mmol \cdot g^{-1}$)	pH_{zpc}	Surface Area ($m^2 \cdot g^{-1}$)
ArS	0.025	0.015	0.093	0.133	0.085	3.6	31.99

3.2. Batch Experiments: Response Surface Methodology

3.2.1. Study of the Parameters: Statistical Study

To optimize cadmium removal efficiency, 15 experiments were conducted simultaneously. The response (Y) represents the amount of cadmium adsorbed. A second-degree linear polynomial regression model was employed to establish the connection between (Y) and the three independent variables along with their interactions [40] (Tong et al., 2011). The following Equation (3) represents this model:

$$Y = a_0 + b_1X_1 + b_2X_2 + b_3X_3 + b_{11}(X_1)^2 + b_{22}(X_2)^2 + b_{33}(X_3)^2 + b_{12}(X_1X_2) + b_{13}(X_1X_3) + b_{23}(X_2X_3) \quad (3)$$

In this equation, a_0 represents the constant term, bi denotes the linear coefficients, and b_{ii} signifies the coefficients for quadratic interactions. The variables X_i (where i = 1, 2, 3) correspond to the independent factors in the process, while Y is the dependent variable representing the amount of cadmium adsorbed.

As shown in Table 3, different combinations of pH, ArS dose, and initial Cd^{2+} concentration were tested to determine adsorption effectiveness. This matrix serves as a foundation for analyzing how variations in pH, ArS dose, and initial Cd^{2+} concentration influence adsorption capacity, supporting RSM optimization of the adsorption process.

Table 3. Experimental design matrix for cadmium adsorption.

Experiment	pH	ArS Dose ($g \cdot L^{-1}$)	$[Cd^{2+}]_i$ ($mg \cdot L^{-1}$)	$q(Cd^{2+})$ ($mg \cdot g^{-1}$)
1	6	2.5	12.5	2.121
2	4	1	12.5	0.951
3	8	4	12.5	2.748
4	6	1	20	1.756
5	8	2.5	20	3.824
6	4	2.5	20	1.678
7	6	4	20	2.898
8	4	2.5	5	0.095
9	6	1	5	0.449
10	8	1	12.5	2.361
11	8	2.5	5	0.863
12	6	2.5	12.5	1.973
13	6	4	5	0.464
14	6	2.5	12.5	2.367
15	4	4	12.5	1.486

$[Cd^{2+}]_i$ is the initial concentration of Cd^{2+} and $q(Cd^{2+})$ represents the Cd^{2+} adsorbed quantity.

3.2.2. Correlation Coefficient

According to the results from the JMP software (17.2 version) and illustrated in Figure 4, a high correlation was found between the predicted (based on the mathematical model) and observed Cd^{2+} adsorption values, having a strong correlation coefficient (R^2 = 0.988), reflecting that the actual experimental results and the model predictions correspond well. This high R^2 value, being close to 1, suggests that the second-degree polynomial model is well-suited for accurately describing the relation between Cd^{2+} adsorption and the selected variables. The combination of a high R^2 value, a low RMSE of 0.1864, and a low *p*-value of 0.0003 demonstrate that the model fits well and is reliable for describing the adsorption process.

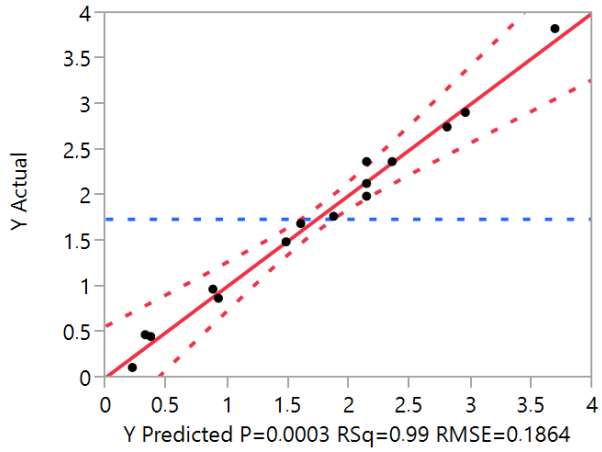

Figure 4. Correlation of predicted and observed values of cadmium adsorption.

3.2.3. Analysis of Variance

In this analysis, ANOVA is applied to examine the statistical significance of the predictive model for cadmium adsorption. This approach determines whether the independent variables (pH, ArS dose, and $[Cd^{2+}]_i$) significantly impact the amount of Cd^{2+} adsorbed. The ANOVA findings of the model are summarized in Table 4. The findings indicate that the model significance is statistically meaningful with 95% confidence in predicting Cd^{2+} adsorption, with a *p*-value corresponding to 0.003 ($p < 0.05$). This result is further supported by an F-ratio of 47.8409, which suggests a significant impact of the independent factors on Cd^{2+} adsorption. Both the low *p*-value and the high F-ratio confirm that the second-degree polynomial model is statistically significant and reliable for predicting cadmium adsorption under the tested conditions.

Table 4. Variance analysis of the adsorbed amount of cadmium.

	Degrees of Freedom	Sum of Squares	Mean Square	F-Ratio
Model	9	14.967247	1.66303	47.8409
Residual	5	0.173808	0.03476	Prob. > F
Total	14	15.141055		0.0003 *

* $p < 0.005$.

3.2.4. Residue Review

Figure 5 presents the residual values from the various experiments. The residual plot shows a dispersed pattern, with residuals randomly scattered around zero and lacking any specific trend. This random distribution suggests that the model accurately describes the data, as it aligns with the expectation that residuals should be randomly distributed

for a well-fitting model. All residual values fall within the range (−0.20, 0.25), indicating the absence of outliers [41]. This narrow range of residuals confirms the reliability of the model and stability in predicting Cd^{2+} adsorption, as extreme values could otherwise signal potential issues with model fit. Overall, the plot supports that the model provides a good fit without systematic errors, making it appropriate for the data.

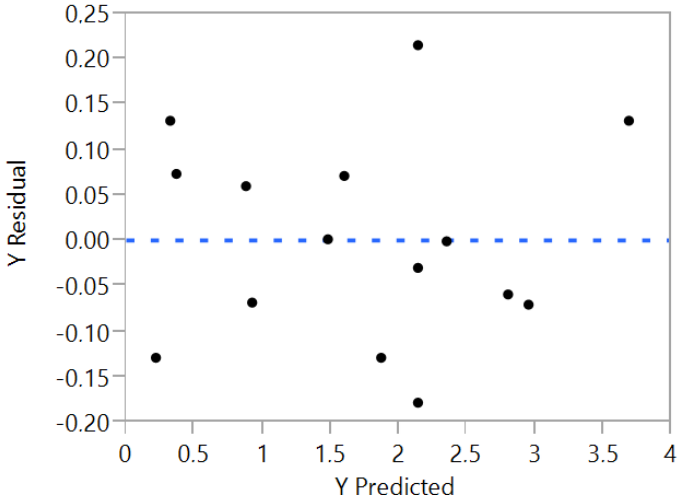

Figure 5. Residual trace of adsorbed cadmium quantity.

3.2.5. Estimation of the Parameters

The *p*-value analysis shows that certain factors significantly influence the amount of Cd^{2+} adsorbed by argan nut shells (ArS), specifically the pH (X_1), adsorbent mass (X_2), initial metal cation concentration (X_3), the quadratic term for concentration (X_3^2), and their interaction terms (X_1X_3, X_2X_3) (Table 5). Each of these terms has a probability value lower than 5%, indicating a statistically significant impact on adsorption [41].

Table 5. Variance analysis of the adsorbed cadmium quantity.

Term	Estimation	Standard Error	t-Ratio	Prob. > |t|
Constant	2.1538235	0.107644	20.01	<0.0001 *
pH (4.8)	0.6982206	0.065918	10.59	0.0001 *
m (1.4)	0.2600368	0.065918	3.94	0.0109 *
cc (5.20)	1.0357132	0.065918	15.71	<0.0001 *
pH × m	−0.036985	0.093222	−0.40	0.7079
pH × cc	0.3443676	0.093222	3.69	0.0141 *
m × cc	0.2820588	0.093222	3.03	0.0292 *
pH × pH	−0.021926	0.097029	−0.23	0.8302
m × m	−0.245206	0.097029	−2.53	0.0527
cc × cc	−0.516706	0.097029	−5.33	0.0031 *

Factors with *p*-values above 0.05 are not statistically significant, indicating minimal effect on the response variable. The final model equation (Equation (4)) incorporates only the significant terms, which include the main effects of pH, ArS mass, and $[Cd^{2+}]_i$, in addition to selected interaction and quadratic terms. The coefficient of each term represents its impact on the predicted cadmium adsorption (Y):

$$Y = 2.154 + 0.698X_1 + 0.26X_2 + 1.0357X_3 - 0.0219X_1^2 - 0.245X_2^2 - 0.517\,X_3^2 - 0.0369\,X_1X_2 + 0.344\,X_1X_3 + 0.282\,X_2X_3 \quad (4)$$

3.2.6. Optimization of the Parameters

This study aimed to identify optimal conditions for maximizing the adsorption of cadmium onto raw argan nut shells. To achieve this, we used numerical optimization based on desirability to identify the best combination of pH, adsorbent mass, and initial [Cd^{2+}]. Figure 6 presents the prediction profiler, which identifies the optimal conditions for maximizing cadmium removal. By maximizing the desirability, the optimal parameters were identified as pH = 8, ArS dose = 3.5 $g{\cdot}L^{-1}$, and [Cd^{2+}] = 20 $mg{\cdot}L^{-1}$. Under these conditions, desirability is close to 1, indicating an optimal solution, with a maximum adsorbed quantity of cadmium of approximately 3.92 $mg{\cdot}g^{-1}$. The prediction profiler also shows that all three parameters (pH, adsorbent mass, and cadmium concentration) positively influence Cd^{2+} adsorption, with higher values generally enhancing the adsorption process.

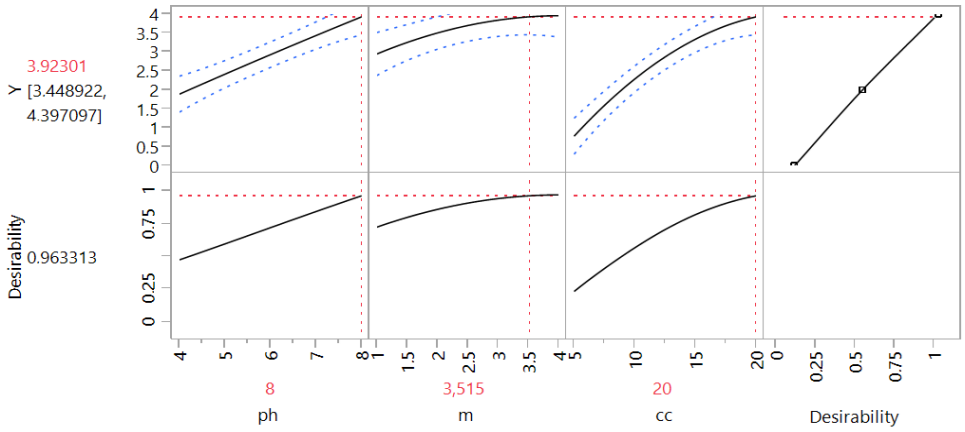

Figure 6. Prediction profiler for optimizing Cd^{2+} adsorption conditions.

3.3. Batch Experiments: Kinetic Study

To comprehend the Cd^{2+} removal kinetics utilizing ArS as a biosorbent, the results were tested with several kinetic models, such as intra-particle diffusion and pseudo-first-order and pseudo-second-order. The study was conducted on ArS under optimal conditions determined by the Box–Behnken design at 25 °C for a duration of 4 h.

Figure 7 illustrates the study of kinetics, showing (a) the adsorption kinetics of Cd^{2+}, (b) the pseudo-first-order model, (c) the pseudo-second-order model, and (d) the intra-particle diffusion model. Analysis of Table 6 and Figure 7 indicates that the pseudo-second-order model most accurately depicts the relationship between t/qt and time. Key parameters, including the coefficient of determination (R^2), estimated equilibrium capacity (q_e), and rate constant (k_2) at $[Cd^{2+}]_i$ = 20 $mg{\cdot}L^{-1}$, can be found in Table 7. The estimated q_e values closely match the practical results, yielding a strong R^2 value ($\geq$0.987) [42], indicating that the pseudo-second-order model delivers a precise description of Cd^{2+} removal by ArS. This implies that the mechanism of adsorption is primarily chemical, involving electron exchange between the adsorbent and adsorbate [43]. In addition, intra-particle transport within the ArS/Cd^{2+} system was assessed using the Weber–Morris equation. Figure 7d shows that cadmium adsorption on argan shells occurs in four distinct phases. The initial phase, marked by a steep slope, indicates rapid adsorption on the external surface. This is followed by three phases with slower diffusion rates, suggesting that intra-particle diffusion contributes to the process of adsorption [44].

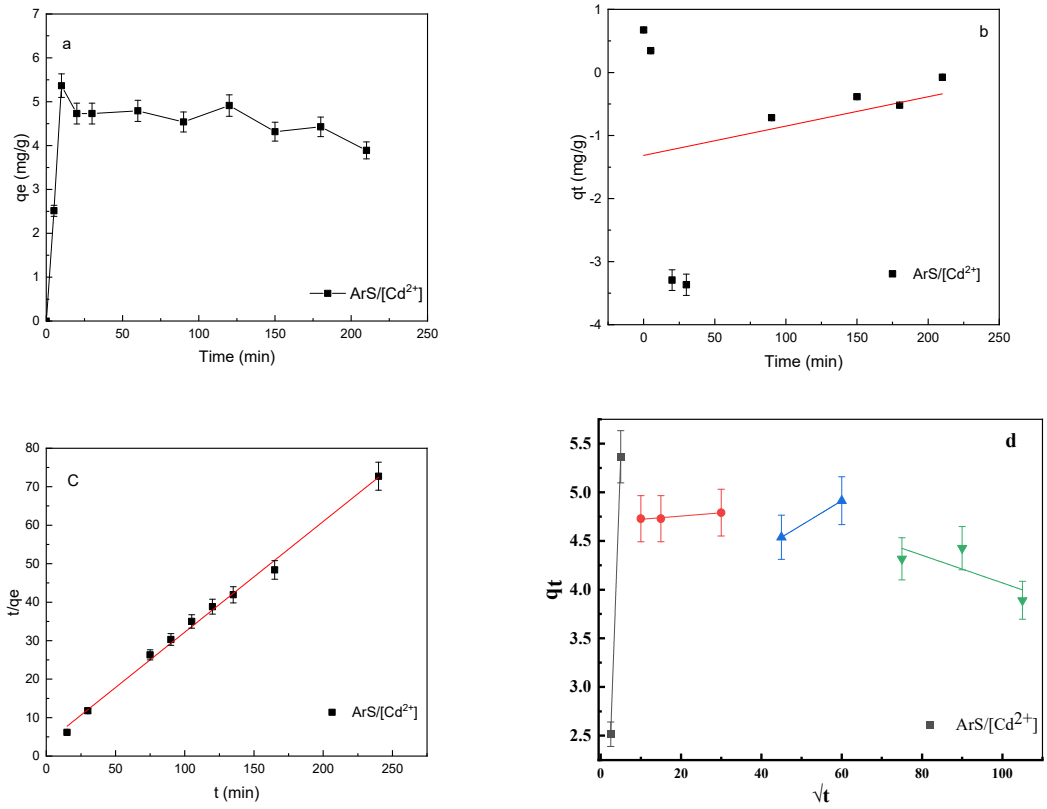

Figure 7. Kinetic study showing: (**a**) the adsorption kinetics of Cd^{2+}, (**b**) the pseudo-first-order model, (**c**) the pseudo-second-order model, and (**d**) the intra-particle diffusion model.

Table 6. Parameters of the kinetic models.

Kinetic Model	Parameters		ArS/Cd^{2+}
Pseudo-first-order [45] (5)	R^2		0.171
	k_1 (min^{-1})		0.373
	q_{etheo} ($mg{\cdot}g^{-1}$)		2.30
	q_{eexp} ($mg{\cdot}g^{-1}$)		4.73
Pseudo-second-order [42]	R^2		0.987
	k_2 (g/mg·min)		−0.065
	q_{etheo} ($mg{\cdot}g^{-1}$)		4.166
	q_{eexp} ($mg{\cdot}g^{-1}$)		4.73
Intra-particle diffusion [44]	Type I	R^2	1
		k_d ($mg{\cdot}g^1$ $min^{0.5}$)	1.14
		I	−0.335
	Type II	R^2	**0.942**
		k_d ($mg{\cdot}g^1$ $min^{0.5}$)	0.003
		I	4.698
	Type III	R^2	1
		k_d (mg/g^1 $min^{0.5}$)	0.025
		I	3.413
	Type IV	R^2	0.566
		k_d (mg/g^1 $min^{0.5}$)	−0.014
		I	5.49

q_t and q_e represent cadmium quantities adsorbed at time (t) and at equilibrium, respectively ($mg \cdot g^{-1}$); t represents the contact time in minutes, K_1, K_2, and K_d are rate constants for pseudo-first-order (min^{-1}), pseudo-second-order (g/mg·min), and intra-particle diffusion ($mg/g \cdot min^{0.5}$), respectively, and I represents the intercept, indicating the boundary layer impact on the process of adsorption ($mg \cdot g^{-1}$).

3.4. Batch Experiments: Isotherms

Figure 8 and Table 8 illustrate the adsorption behavior of Cd^{2+} on ArS and the corresponding isotherm model parameters. The plots in Figure 8 represent the Langmuir (a), Freundlich (b), Temkin (c), and Dubinin–Radushkevich (d) isotherm models. The Langmuir equilibrium constants were calculated through the graphical representation of $1/q_e$ against $1/C_e$, according to the linear representation of the model of Langmuir. Since R^2 is equal to 0.99, close to 1, the model of Langmuir fits the data quite well in contrast to the Freundlich isotherm ($R^2 = 0.859$), highlighting the accuracy of Langmuir model. The Qads value from the Langmuir model (4 $mg \cdot g^{-1}$) aligns with the experimental adsorption capacity (3.26 $mg \cdot g^{-1}$) [46]. The dimensionless constant $R_L = 0.05$ (ranging between 0 and 1) suggests that the adsorption process is favorable [47]. As the concentration increases, R_L approaches zero, suggesting the adsorption process is becoming irreversible [48]. The $\log(q_e)$ versus $\log(C_e)$ figure was used to determine the Freundlich constants yielding lower R^2 (0.859) than the Langmuir isotherm. The $1/n_F$ value of 0.33 (less than 1) implies typical adsorption behavior under the Freundlich model [49]. Figure 8c illustrates the Temkin isotherm (Q_e vs. ln C_e), which describes adsorption on heterogeneous surfaces. It describes the decline in adsorption energy as surface coverage increases and assumes uniform binding energy distribution [50]. The R^2 of 0.902 indicates a moderate fit, with constants $B_T = 0.718$ $J \cdot mol^{-1}$ and $K_T = 1.432$ L/g^{-1} reflecting the heat of adsorption. The Dubinin–Radushkevich model, as illustrated in Figure 8d, achieves a strong correlation ($R^2 = 0.984$), suggesting a reliable fit with experimental data. The computed energy E = 3.488 $KJ \cdot mol^{-1}$, below 8 $KJ \cdot mol^{-1}$, implies that the Cd^{2+} sorption on ArS is mostly physical [50]. Table 8 summarizes these findings, underscoring the Langmuir model's superior fit ($R^2 = 0.99$) compared to the other models. The Dubinin–Radushkevich model follows closely with $R^2 = 0.984$, while the Freundlich and Temkin models show moderate correlations ($R^2 = 0.859 = 0.859$ and 0.902, respectively).

Q_e and q_m represent the quantity of adsorbate adsorbed under equilibrium conditions and the maximum adsorption capacity, respectively, both measured in milligrams per gram ($mg \cdot g^{-1}$); C_e denotes the equilibrium concentration of the unadsorbed adsorbate in the liquid phase ($mg \cdot L^{-1}$); T represents the absolute temperature in Kelvin; R denotes the universal gas constant, valued at 8.314 J/mol·K; β represents a constant from the Dubinin–Radushkevich isothermal model that relates to adsorption capacity. It represents the average free energy of adsorption for a single molecule as it moves from an infinite distance to the solid surface. $E = 1/\sqrt{2\beta}$ is the formula used to determine the free energy. K_L, K_F, and K_T are constants corresponding to the Langmuir ($L \cdot mg^{-1}$), Freundlich ($mg^{(1-n)}L^n \cdot g^{-1}$), and Temkin ($L \cdot mg^{-1}$) models, respectively; R_L is the equilibrium factor, often known as the dimensionless separation factor and expressed as $R_L = 1/(1 + K_L \cdot C_0)$ [52]; BT represents the constant related to the heat of adsorption, defined by the equation $B_T = R \cdot T/K_T$ [52]; b_T represents the isothermal constant of Temkin and 1/nf represents the heterogeneity factor. Table 8 compares the adsorption capacities of various lignocellulosic biosorbents, showing that raw argan shells, with a capacity of 4 mg/g at pH 8, performed better than some biosorbents such as cashew activated carbon (CAC) (2.87 $mg \cdot g^{-1}$) [19] and rice husk ash (3.04 $mg \cdot g^{-1}$). However, walnut shells (4.36 $mg \cdot g^{-1}$) and raw walnut shells (5.38 $mg \cdot g^{-1}$) [15] had higher capacities. This analysis highlights that, while ArS shows significant adsorption potential, certain materials like walnut shells may offer superior performance.

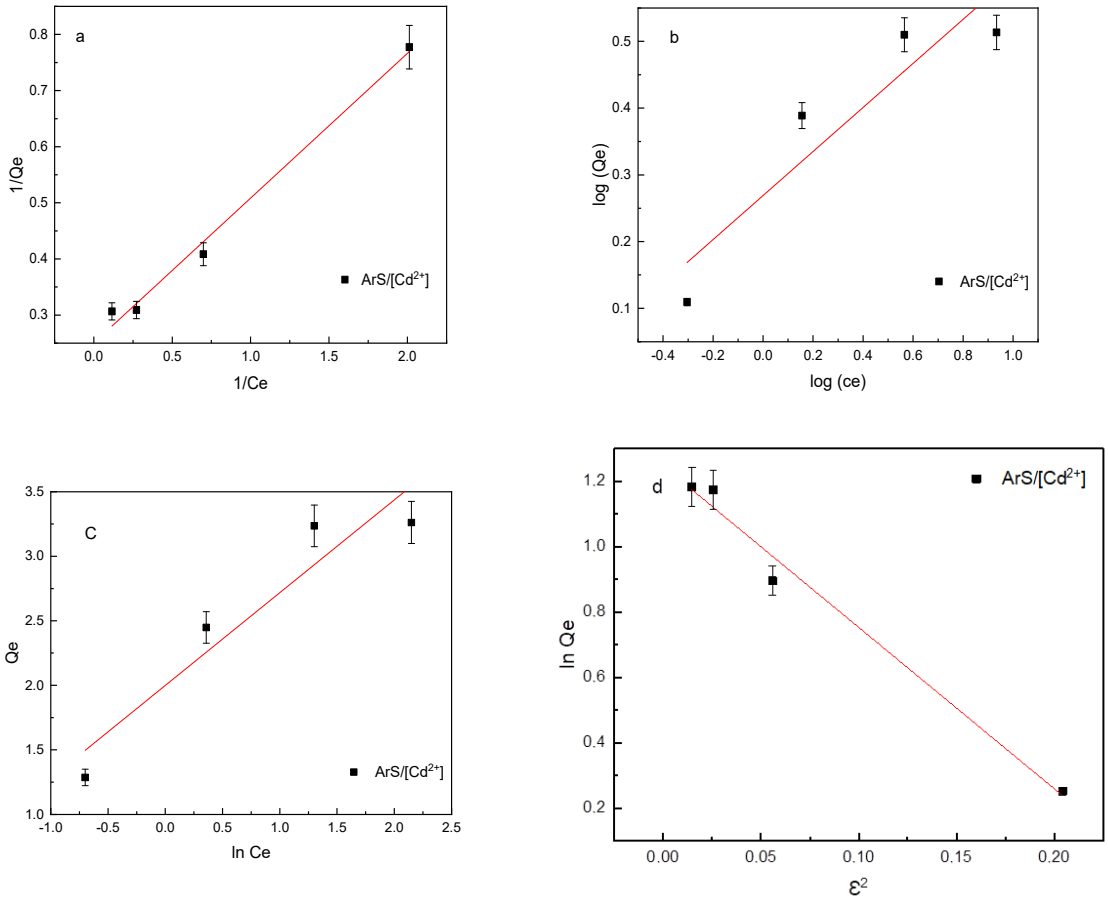

Figure 8. Plots of isothermal models by Langmuir (**a**), Freundlich (**b**), Temkin (**c**), as well as Dubinin–Radushkevich (**d**) for Cd^{2+} adsorption on ArS.

Table 7. Isotherm parameters.

Isotherms	Parameters	Values
Langmuir	q_m ($mg \cdot g^{-1}$)	4
	K_L ($L \cdot g^{-1}$)	0.91
	R_L	0.0521
	R^2	0.99
Freundlich [50]	$1/n_f$	0.33
	K_f ($mg^{(1-n)}L^n \cdot g^{-1}$)	1.8516
	R^2	0.859
Temkin	B_T ($J \cdot mol^{-1}$)	0.718
	K_T ($L \cdot g^{-1}$)	1.432
	R^2	0.902
	b_T (J/molK)	1731.13
Dubinin–Radushkevich [51]	E ($KJ \cdot mol^{-1}$)	3.488
	Q_e ($mg \cdot g^{-1}$)	3.525
	β (J^2/mol^2)	4.933
	R^2	0.984

Table 8. Comparison of cadmium capacities of adsorption on various lignocellulosic adsorbents.

Samples	Adsorption Capacity ($mg \cdot g^{-1}$)	pH	Reference
Pine bark (P. pinaster Ait)	3.23	3.4	[14]
Walnut shells	4.36	6	[20]
Cashew activated carbon	2.87	5	[18]
Raw walnut shells (RWS)	5.38	6	[15]
Coffee beans	3.80	8	[16]
Ash produced from rice husks	3.04	6	[19]
Rice-hull-derived AC	2.49	4.5	[17]
Raw argan shells	4	8	This work

3.5. Batch Experiments: Thermodynamic Parameters

The experimental temperature range for this study was between 25 °C and 65 °C, with 175 mg of ArS used in 50 mL of a 20 $mg \cdot L^{-1}$ cadmium mixture. Notably, the adsorption capacity of Cd^{2+} was augmented from 3.45 $mg \cdot g^{-1}$ at 25 °C to 4.74 $mg \cdot g^{-1}$ at 65 °C. To assess the spontaneity, feasibility, and nature of the adsorbate and adsorbent, different thermodynamic factors of the reaction, namely, entropy (ΔS°), enthalpy (ΔH°), and Gibbs free energy (ΔG°), were determined by using Equations (5) and (6) [53]:

$$\ln(K_d) = \Delta S^\circ / R - \Delta H^\circ / RT \quad (5)$$

$$\Delta G^o = -RT \ln(K_d) \quad (6)$$

Using T as the Kelvin temperature and R as the gas constant, K_d may be found using qe/Ce, and ΔH° and ΔS° can be found through the graphical representation of $\ln(K_d)$ vs. T^{-1}.

The thermodynamic parameters for Cd^{2+} adsorption on argan shells (Table 9) reveal key insights. The Gibbs free energy (ΔG°) values shift from positive at lower temperatures (2.26 $KJ \cdot mol^{-1}$ at 298.15 K) to negative (−0.43 $KJ \cdot mol^{-1}$ at 338.15 K), showing that, at lower temperatures, the process is not spontaneous but becomes spontaneous as temperature increases, suggesting that higher temperatures favor adsorption. The positive enthalpy (ΔH° = 20.26 $KJ \cdot mol^{-1}$) shows that the process is endothermic [53], implying that energy input is needed for adsorption, which is consistent with a chemical adsorption mechanism where Cd^{2+} ions likely form strong interactions with the argan shell surface. The positive entropy (ΔS° = 60.36 J/mol·K) suggests a dissociative mechanism, where the disorder at the solid–liquid interface increases as ions interact with the adsorption sites [54]. Together, these observations indicate that the adsorption of Cd^{2+} onto ArS is endothermic, likely chemical, and is enhanced by higher temperatures, with a dissociative mechanism at play.

Table 9. Cd^{2+} adsorption thermodynamics on ArS.

T	ΔG° ($KJ \cdot mol^{-1}$)	ΔH° ($KJ \cdot mol^{-1}$)	ΔS° (J/mol·K)	R^2
298.15	2.26	20.26	60.36	0.913
308.15	1.43			
323.15	1.24			
338.15	−0.43			

3.6. Desorption Study of Cd^{2+} from ArS

The desorption study is a crucial step to evaluate the reusability of the adsorbent and the potential for cost-effective and sustainable heavy metal removal in water treatment

processes [55]. Cd^{2+} desorption was carried out under optimum conditions. After equilibration, ArS was filtered and rinsed with 10 mL of distilled water. It was then added to various acid solutions (1 M HCl, 1 M HNO_3, and 1 M CH_3COOH) to evaluate the efficiency of the different eluents. Metal ion desorption was carried out over a 12 h period. Cd^{2+} desorption (DP) is calculated as follows:

$$DP = \frac{C_{de}\left(Cd^{2+}\right)}{C_{ad}\left(Cd^{2+}\right)} \times 100 \quad (7)$$

where C_{ad} represents $[Cd^{2+}]$ adsorbed on the ArS adsorbent and Cde corresponds to $[Cd^{2+}]$ desorbed by the various acid solutions.

The results of Cd^{2+} desorption are shown in Figure 9. Among the acidic agents tested, HCl proved the most effective, with a desorption rate of 90.02%, followed by HNO_3 with 76.65%, and finally CH_3COOH with 71.59%. The desorption efficiencies with the different acids can be correlated with their relative acid strengths. HCl, being a strong monoprotic acid, is fully dissociated in solution, generating a high H^+ ion concentration, which interferes with the interaction between Cd^{2+} and the ArS surface. HNO_3, another strong acid, was found to have a somewhat lower efficiency, likely due to the difference in ionic interactions with Cd^{2+}. CH_3COOH, being a weak acid, might have formed more stable complexes with Cd^{2+} and thus reduced its desorption efficiency.

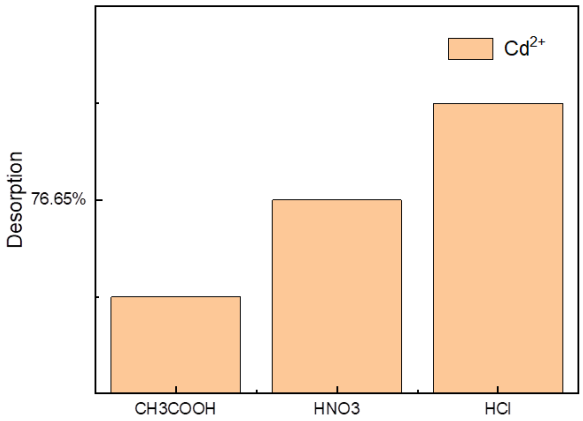

Figure 9. Cd^{2+} desorption using different acid solutions (HCl, HNO_3, and CH_3COOH).

3.7. Proposed Adsorption Mechanisms

Effective removal of impurities from aqueous solutions requires understanding the mechanisms underlying solute adsorption on solid surfaces. This adsorption can involve ionic interactions between opposite charges, such as chemical bonding, H bonding, dipole–dipole, dipole-induced dipole, and ion exchange. FTIR is a valuable technique for defining the ArS chemical structure, which primarily consists of cellulose, hemicellulose, lignin, and ash. It has proven effective as a biosorbent for cadmium ions (Cd^{2+}) in solution. FTIR analysis before and after adsorption (Figure 10) reveals significant shifts in the bands of specific functional groups after Cd^{2+} adsorption, indicating modifications to both the surface characteristics and functional groups of the biosorbent. These shifts likely result from changes in counterions related to hydroxylate and carboxylate anions, suggesting that hydroxyl and carboxyl functional sites are key in Cd^{2+} biosorption [20]. Experimental findings demonstrate that optimal adsorption of Cd^{2+} onto the ArS surface occurs at pH equal to 8, greater than the zero point of charge (pH_{zpc} = 3.6) [26]. Above this pH, the ArS surface becomes negatively charged because of the deprotonation of cellulose-OH and lignin-OH sites, facilitated by OH^- anions in the solution. This negative charge enhances

the attraction of Cd^{2+} cations [56]. Boehm theoretical analysis suggests that acidic groups predominate on the ArS surface compared to basic groups, highlighting oxygen-based reactive sites contributing to the adsorption process. This outcome agrees with the FTIR examination, confirming the roles of hydroxyl and carboxyl groups in Cd^{2+} biosorption.

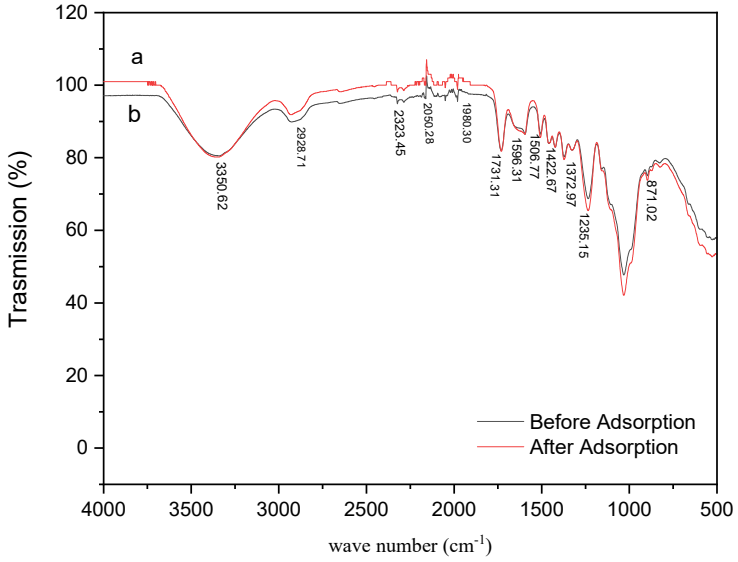

Figure 10. ArS FTIR spectra.

Figure 11 illustrates the adsorption mechanism of Cd^{2+} on cellulose and lignin. In lignin, deprotonated phenolic hydroxides interact with Cd^{2+}, forming stable complexes, while in cellulose, the deprotonation of hydroxyl groups creates active sites that coordinate with Cd^{2+}. This highlights the significant roles of surface functional groups and pH in driving effective adsorption. The FTIR results, which show shifts in functional group bands after Cd^{2+} adsorption, further support these interactions, with hydrogen bonding and coordination bonds playing central roles.

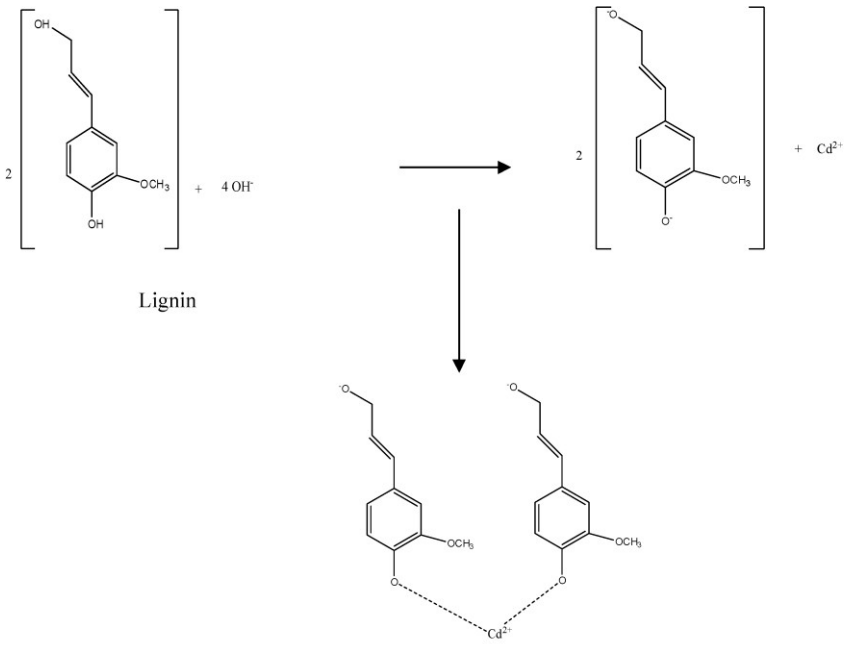

Figure 11. *Cont.*

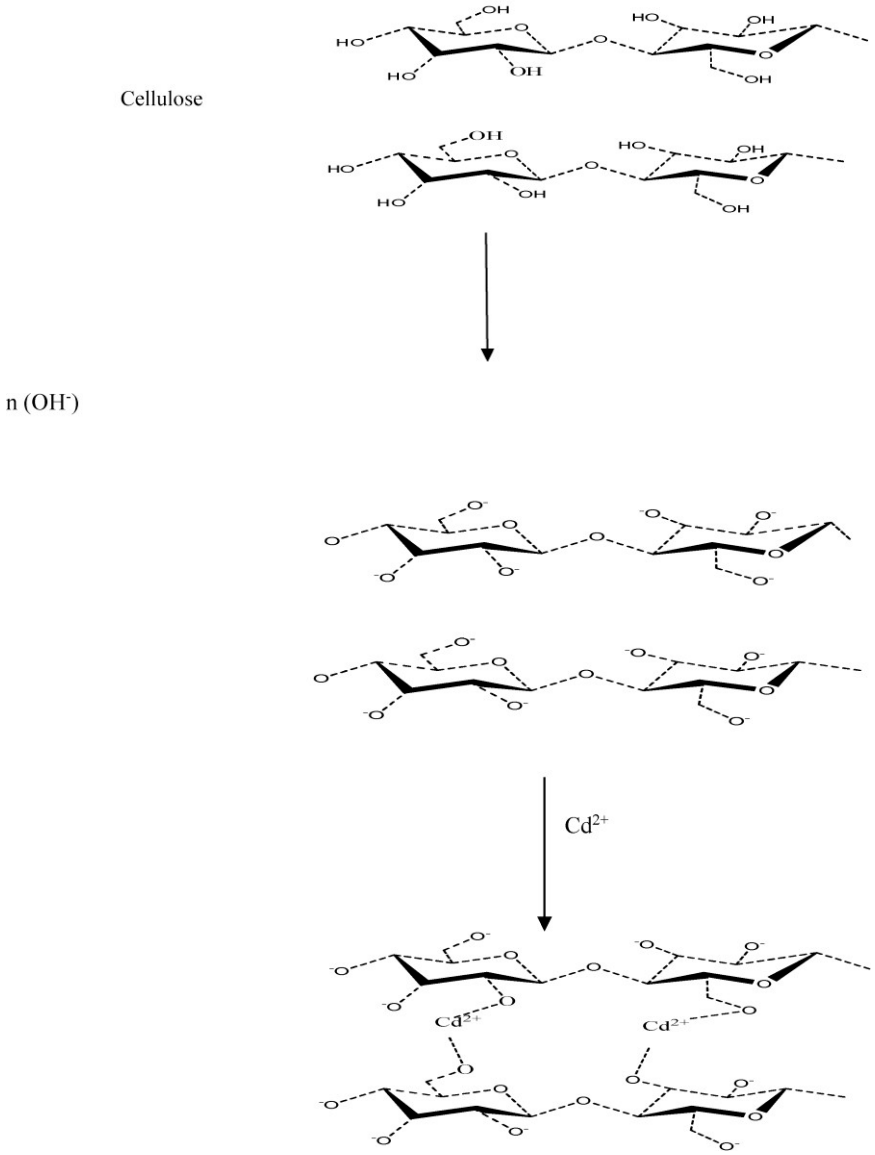

Figure 11. Adsorption mechanism of Cd^{2+} on cellulose and lignin.

4. Conclusions

Cd^{2+} ion removal from aqueous solutions utilizing ArS as an adsorbent was analyzed through various kinetic models, isotherms, and the response surface methodology in conjunction with the Box–Behnken design. This approach helped identify the optimal conditions for adsorption, which involves pH, ArS dosage, and $[Cd^{2+}]_i$, as well as the factors influencing adsorption capacity. The optimization results indicate that, to achieve an adsorbed amount of 3.92 mg, the ideal parameters are a pH of 8, an ArS mass of 3.5 $g \cdot L^{-1}$, and an initial $[Cd^{2+}]_i$ = 20 $mg \cdot L^{-1}$. The isotherm analysis revealed that the Langmuir model, with an R^2 of 0.96, provided the best fit, indicating that adsorption takes place as a single layer on a homogeneous surface. Additionally, the adsorption kinetics demonstrated that metal ion binding happens rapidly in the initial phase, gradually slowing down as intra-particle diffusion takes effect. Furthermore, the pseudo-second-order kinetic model showed remarkable agreement with the findings from the experiment (R^2 = 0.987), confirming the model's suitability for describing the Cd^{2+} adsorption process.

Author Contributions: Conceptualization, F.-Z.A.; Methodology, F.-Z.A., M.B. (Maria Benbouzid), K.B., H.N., M.B. (Meryem Bensemlali), N.L. and S.E.H.; Software, F.-Z.A., M.B. (Maria Benbouzid), K.B., H.N., M.B. (Meryem Bensemlali), N.L. and S.E.H.; Validation, F.-Z.A., M.B. (Maria Benbouzid), K.B., H.N., M.B. (Meryem Bensemlali), N.L. and S.E.H.; Formal analysis, F.-Z.A., M.B. (Maria Benbouzid), K.B., H.N., M.B. (Meryem Bensemlali), N.L. and S.E.H.; Investigation, F.-Z.A., M.B. (Maria Benbouzid), K.B., H.N., M.B. (Meryem Bensemlali), N.L. and S.E.H.; Resources, F.-Z.A., M.B. (Maria Benbouzid), K.B., H.N., M.B. (Meryem Bensemlali), N.L. and S.E.H.; Data curation, F.-Z.A., M.B. (Maria Benbouzid), K.B., H.N., N.L. and S.E.H.; Writing—original draft, F.-Z.A., M.B. (Maria Benbouzid), H.N., M.B. (Meryem Bensemlali), N.L. and S.E.H.; Writing—review & editing, F.-Z.A., H.N., N.L. and S.E.H.; Visualization, F.-Z.A., H.N., N.L. and S.E.H.; Supervision, N.L. and S.E.H. All authors have read and agreed to the published version of the manuscript.

Funding: The authors would like to thank all of the project participants "Wastewater reuse in countries with high water stress—challenges and opportunities" for their scientific support and their comments, which significantly improved the manuscript. Financial support from the Swedish Research Council VR (Grant No. 2018-03476), is gratefully acknowledged.

Data Availability Statement: The original contributions presented in this study are included in the article. Further inquiries can be directed to the corresponding author.

Conflicts of Interest: The authors declare no conflict of interest.

References

1. Hamid, N.H.A.; Rushdan, A.I.; Nordin, A.H.; Husna, S.M.N.; Faiz Norrrahim, M.N.; Knight, V.F.; Tahir, M.I.H.M.; Li, G.X.; Quan, T.L.; Abdullah, A.M.; et al. A state-of-art review on the sustainable technologies for cadmium removal from wastewater. *Water Reuse* **2024**, *14*, 312–341. [CrossRef]
2. Liang, Q.; Luo, H.; Geng, J.; Chen, J. Facile one-pot preparation of nitrogen-doped ultra-light graphene oxide aerogel and its prominent adsorption performance of Cr(VI). *Chem. Eng. J.* **2018**, *338*, 62–71. [CrossRef]
3. Fulke, A.B. Understanding heavy metal toxicity: Implications on human health, marine ecosystems and bioremediation strategies. *Mar. Pollut. Bull.* **2024**, *206*, 116707. [CrossRef]
4. Guarín-Romero, J.R.; Rodríguez-Estupiñán, P.; Giraldo, L.; Moreno-Piraján, J.C. Simple and Competitive Adsorption Study of Nickel(II) and Chromium(III) on the Surface of the Brown Algae Durvillaea antarctica Biomass. *ACS Omega* **2019**, *4*, 18147–18158. [CrossRef]
5. Dhanda, A.; Lamba, R.; Deepika, S.; Prakash, R. *Cadmium in Environment—An Overview*; Springer: Berlin/Heidelberg, Germany, 2024; pp. 3–20. [CrossRef]
6. Kouzbour, S.; Gourich, B.; Gros, F.; Vial, C.; Allam, F.; Stiriba, Y. Comparative analysis of industrial processes for cadmium removal from phosphoric acid: A review. *Hydrometallurgy* **2019**, *188*, 222–247. [CrossRef]
7. Suciu, N.A.; De Vivo, R.; Rizzati, N.; Capri, E. Cd content in phosphate fertilizer: Which potential risk for the environment and human health? *Curr. Opin. Environ. Sci. Health* **2022**, *30*, 100392. [CrossRef]
8. Kubier, A.; Wilkin, R.T.; Pichler, T. Cadmium in soils and groundwater: A review. *Appl. Geochem. J. Int. Assoc. Geochem. Cosmochem.* **2019**, *108*, 104388. [CrossRef]
9. Sadeek, S.A.; Negm, N.A.; Hefni, H.H.H.; Wahab, M.M.A. Metal adsorption by agricultural biosorbents: Adsorption isotherm, kinetic and biosorbents chemical structures. *Int. J. Biol. Macromol.* **2015**, *81*, 400–409. [CrossRef]
10. Godt, J.; Scheidig, F.; Grosse-Siestrup, C.; Esche, V.; Brandenburg, P.; Reich, A.; Groneberg, D.A. The toxicity of cadmium and resulting hazards for human health. *J. Occup. Med. Toxicol.* **2006**, *1*, 22. [CrossRef]
11. Rashid, A.; Bhatti, H.N.; Iqbal, M.; Noreen, S. Fungal biomass composite with bentonite efficiency for nickel and zinc adsorption: A mechanistic study. *Ecol. Eng.* **2016**, *91*, 459–471. [CrossRef]
12. Qasem, N.; Mohammed, R.; Lawal, D. Removal of heavy metal ions from wastewater: A comprehensive and critical review. *NPJ Clean Water* **2021**, *4*, 36. [CrossRef]
13. Nascimento, T.L.; Oliveira, K.F.; Junior, J.O.; Pimenta, A.S.; Melo, D.M.; Melo, M.A.; Braga, R.M. Biosorption of nickel and cadmium using *Pachira aquatica* Aubl. peel biochar. *Sci. Rep.* **2024**, *14*, 5086. [CrossRef]
14. Cutillas-Barreiro, L.; Ansias-Manso, L.; Fernández-Calviño, D.; Arias-Estévez, M.; Nóvoa-Muñoz, J.C.; Fernández-Sanjurjo, M.J.; Álvarez-Rodríguez, E.; Núñez-Delgado, A. Pine bark as bio-adsorbent for Cd, Cu, Ni, Pb and Zn: Batch-type and stirred flow chamber experiments. *J. Environ. Manag.* **2014**, *144*, 258–264. [CrossRef]
15. Gondhalekar, S.C.; Shukla, S.R. Biosorption of cadmium metal ions on raw and chemically modified walnut shells. *Environ. Prog. Sustain. Energy* **2015**, *34*, 1613–1619. [CrossRef]

16. Kaikake, K.; Hoaki, K.; Sunada, H.; Dhakal, R.; Baba, Y. Removal Characteristics of Metal Ions Using Degreased Coffee Beans: Adsorption Equilibrium of Cadmium(II). *Bioresour. Technol.* **2007**, *98*, 2787–2791. [CrossRef]
17. Lee, S.-M.; Lalhmunsiama, C.S.-I.; Tiwari, D. Manganese and iron oxide immobilized activated carbons precursor to dead biomasses in the remediation of cadmium-contaminated waters. *Environ. Sci. Pollut. Res. Int.* **2013**, *20*, 7464–7477. [CrossRef]
18. N'goran, P.D.A.; Diabaté, D.; Yao, K.M.; Berenger, K.; Gnonsoro, U.; Kinimo, K.; Trokourey, A. Lead and cadmium removal from natural freshwater using mixed activated carbons from cashew and shea nut shells. *Arab. J. Geosci.* **2018**, *11*, 498. [CrossRef]
19. Srivastava, N.K.; Majumder, C.B. Novel biofiltration methods for the treatment of heavy metals from industrial wastewater. *J. Hazard. Mater.* **2008**, *151*, 1–8. [CrossRef]
20. Kamsonlian, S.; Suresh, S.; Majumder, C.B.; Chand, S. Biosorption of As(III) from contaminated water onto low cost palm bark biomass. *Int. J. Curr. Eng. Technol.* **2012**, *2*, 153–158.
21. Weshahy, A.R.; Sakr, A.K.; Gouda, A.A.; Atia, B.M.; Somaily, H.H.; Hanfi, M.Y.; Gado, M.A. Selective re-covery of cadmium, cobalt, and nickel from spent Ni–Cd batteries using Adogen® 464 and mesoporous silica deriva-tives. *Int. J. Mol. Sci.* **2022**, *23*, 8677. [CrossRef]
22. Najah El Idrissi, A.; Benbrahim, M.; Rassai, N. Effect of the particle size argan nut shell (ANS) biomass on combustion parameters in stirling engine in Morocco. *Results Eng.* **2023**, *18*, 101202. [CrossRef]
23. Boundati, Y.; Ziat, K.; Naji, A.; Saidi, M.; Rghioui, L. Copper biosorption on argan nut shell: Kinetic and thermodynamic studies. *Int. J. Adv. Res.* **2018**, *6*, 300–309. [CrossRef]
24. Millett, M.A.; Baker, A.J.; Satter, L.D. Physical and chemical pretreatments for enhancing cellulose saccharification. *Biotechnol. Bioeng. Symp.* **1976**, *6*, 125–153.
25. Benadjemia, M.; Milliere, L.; Reinert, L.; Benderdouche, N.; Duclaux, L. Preparation, characterization and Meth-ylene Blue adsorption of phosphoric acid activated carbons from globe artichoke leaves. *Fuel Energy Abstr.* **2011**, *92*, 1203–1212. [CrossRef]
26. Bencheikh, I.; Azoulay, K.; Mabrouki, J.; El Hajjaji, S.; Moufti, A.; Labjar, N. The use and the performance of chemically treated artichoke leaves for textile industrial effluents treatment. *Chem. Data Collect.* **2021**, *31*, 100597. [CrossRef]
27. Es-said, A.; Hamdaoui, L.; El Moussaouiti, M.; Bchitou, R. Esterification optimization of cellulose with p-Iodobenzoyl chloride using experimental design method. *J. Polym. Res.* **2019**, *26*, 237. [CrossRef]
28. Benallou Benzekri, M.; Benderdouche, N.; Bestani, B.; Douara, N.; Duclaux, L. Valorization of olive stones into a granular activated carbon for the removal of Methylene blue in batch and fixed bed modes. *J. Mater. Environ. Sci.* **2018**, *9*, 272–284. [CrossRef]
29. Olabinjo, O.O. Response Surface Techniques as an Inevitable Tool in Optimization Process. In *Response Surface Methods—Theory, Applications and Optimization Techniques*; IntechOpen: London, UK, 2024. [CrossRef]
30. Duan, R.; Fedler, C.; Jiao, X. Adsorption of pyridine from aqueous solutions onto polyaluminium chloride and anionic polyacrylamide water treatment residuals. *Water Sci. Technol.* **2021**, *83*, 1753–1763. [CrossRef]
31. Güray, T.; Menevşe, B.; Yavuz, A.A. Determination of optimization parameters based on the Box-Behnken design for cloud point extraction of quinoline yellow using Brij 58 and application of this method to real samples. *Spectrochim. Acta Part A Mol. Biomol. Spectrosc.* **2020**, *243*, 118800. [CrossRef]
32. Zhuang, J.; Li, M.; Pu, Y.; Ragauskas, A.J.; Yoo, C.G. Observation of potential contaminants in processed biomass using fourier transform infrared spectroscopy. *Appl. Sci.* **2020**, *10*, 4345. [CrossRef]
33. Olsson, A.-M.; Salmén, L. The association of water to cellulose and hemicellulose in paper examined by FTIR spectroscopy. *Carbohydr. Res.* **2024**, *339*, 813–818. [CrossRef]
34. Paiva, M.; Ammar, I.; Campos, A.R.; Cheikh, R.; Cunha, A. Alfa fibres: Mechanical, morphological and interfacial characterization. *Compos. Sci. Technol.* **2007**, *67*, 1132–1138. [CrossRef]
35. Arrakhiz, F.Z.; El Achaby, M.; Malha, M.; Bensalah, M.O.; Fassi-Fehri, O.; Bouhfid, R.; Benmoussa, K.; Qaiss, A. Mechanical and thermal properties of natural fibers reinforced polymer composites: Doum/low density polyethylene. *Mater. Des.* **2013**, *43*, 200–205. [CrossRef]
36. Liu, D.; Han, G.; Huang, J.; Zhang, Y. Composition and structure study of natural Nelumbo nucifera fiber. *Carbohydr. Polym.* **2009**, *75*, 39–43. [CrossRef]
37. Sen, T.K. Agricultural Solid Wastes Based Adsorbent Materials in the Remediation of Heavy Metal Ions from Water and Wastewater by Adsorption: A Review. *Molecules* **2023**, *28*, 5575. [CrossRef]
38. Salleh, M.A.M.; Mahmoud, D.K.; Karim, W.A.W.A.; Idris, A. Cationic and anionic dye adsorption by agricultural solid wastes: A comprehensive review. *Desalination* **2011**, *280*, 1–13. [CrossRef]
39. Benbouzid, M.; Azoulay, K.; Bencheikh, I.; Al-Jadab, N.; Bensemlali, M.; Aarfane, A.; Nasrellah, H.; El Hajjaji, S.; Labjar, N. Evaluation of natural porous material as media filters for domestic wastewater treatment using infiltration percolation process. *Euro-Mediterr. J. Environ. Integr.* **2024**, 1–16. [CrossRef]
40. Tong, K.S.; Kassim, M.J.; Azraa, A. Adsorption of copper ion from its aqueous solution by a novel biosorbent Uncaria gambir: Equilibrium, kinetics, and thermodynamic studies. *Chem. Eng. J.* **2011**, *170*, 145–153. [CrossRef]

41. Fadil, M.; Farah, A.; Ihssane, B.; Haloui, T.; Rachiq, S. Optimisation des paramètres influençant l'hydrodistillation de Rosmarinus officinalis L. par la méthodologie de surface de réponse Optimization of parameters influencing the hydrodistillation of Rosmarinus officinalis L. by response surface methodology. *J. Mater. Environ. Sci.* **2015**, *6*, 2346–2357.
42. Azoulay, K.; Bencheikh, I.; Mabrouki, J.; Samghouli, N.; Moufti, A.; Dahchour, A.; El Hajjaji, S. Adsorption mecha-nisms of azo dyes binary mixture onto different raw palm wastes. *Int. J. Environ. Anal. Chem.* **2023**, *103*, 1633–1652. [CrossRef]
43. Vishan, I.; Saha, B.; Sivaprakasam, S.; Kalamdhad, A. Evaluation of Cd(II) biosorption in aqueous solution by using lyophilized biomass of novel bacterial strain Bacillus badius AK: Biosorption kinetics, thermodynamics and mechanism. *Environ. Technol. Innov.* **2019**, *14*, 100323. [CrossRef]
44. Ma, P.; Ma, M.; Wu, J.; Qian, Y.; Wu, D.; Zhang, X. The effect of plastic on performance of activated carbon and study on adsorption of methylene blue. *J. Mater. Res.* **2019**, *34*, 3040–3049. [CrossRef]
45. Abdolali, A.; Ngo, H.H.; Guo, W.; Lu, S.; Chen, S.-S.; Nguyen, N.C.; Zhang, X.; Wang, J.; Wu, Y. A breakthrough biosorbent in removing heavy metals: Equilibrium, kinetic, thermodynamic and mechanism analyses in a lab-scale study. *Sci. Total Environ.* **2016**, *542*, 603–611. [CrossRef]
46. Putro, J.N.; Kurniawan, A.; Ismadji, S.; Ju, Y.-H. Nanocellulose based biosorbents for wastewater treatment: Study of isotherm, kinetic, thermodynamic and reusability. *Environ. Nanotechnol. Monit. Manag.* **2017**, *8*, 134–149. [CrossRef]
47. Kluczka, J.; Pudło, W.; Krukiewicz, K. Boron adsorption removal by commercial and modified activated carbons. *Chem. Eng. Res. Des.* **2019**, *147*, 30–42. [CrossRef]
48. Kavakli, C.; Akkaş Kavaklı, P.; Turan, B.; Hamurcu, A.; Güven, O. Quaternized dimethylaminoethyl methacrylate strong base anion exchange fibers for As(V) adsorption. *Radiat. Phys. Chem.* **2014**, *102*, 84–95. [CrossRef]
49. Abid, M.; Niazi, N.K.; Bibi, I.; Farooqi, A.; Ok, Y.S.; Kunhikrishnan, A.; Ali, F.; Ali, S.; Igalavithana, A.D.; Arshad, M. Arsenic(V) biosorption by charred orange peel in aqueous environments. *Int. J. Phytoremediat.* **2016**, *18*, 442–449. [CrossRef]
50. Foo, K.Y.; Hameed, B.H. Insights into the modeling of adsorption isotherm systems. *Chem. Eng. J.* **2010**, *156*, 2–10. [CrossRef]
51. Yang, Z.; Gluesenkamp, K.R.; Frazzica, A. Equilibrium vapor pressure properties for absorbent and adsorbent materials. *Int. J. Refrig.* **2021**, *124*, 134–166. [CrossRef]
52. Shehu, A.; Ibrahim, M.B. Equilibrium Adsorption Isotherm of Methylene Blue and Rhodamine B Using Shea Butter Leaves as a Low-Cost Adsorbent. *Appl. J. Environ. Eng. Sci.* **2023**, *9*. [CrossRef]
53. Zhang, M.; Wang, H. Raw and calcination-modified coal waste as adsorbents to remove cadmium from simulated mining wastewater. *Int. J. Environ. Sci. Technol.* **2014**, *11*, 987–996. [CrossRef]
54. Gupta, A.; Sharma, V.; Mishra, P.K.; Ekielski, A. A Review on Polyacrylonitrile as an Effective and Economic Constituent of Adsorbents for Wastewater Treatment. *Molecules* **2022**, *27*, 8689. [CrossRef] [PubMed]
55. Isaac, R.; Siddiqui, S.; Aldosari, O.F.; Uddin, M.K. Magnetic biochar derived from Juglans regia for the adsorption of Cu^{2+} and Ni^{2+}: Characterization, modelling, optimization, and cost analysis. *J. Saudi Chem. Soc.* **2023**, *27*, 101749. [CrossRef]
56. Al-Ghouti, M.A.; Li, J.; Salamh, Y.; Al-Laqtah, N.; Walker, G.; Ahmad, M.N.M. Adsorption mechanisms of re-moving heavy metals and dyes from aqueous solution using date pits solid adsorbent. *J. Hazard. Mater.* **2010**, *176*, 510–520. [CrossRef] [PubMed]

Disclaimer/Publisher's Note: The statements, opinions and data contained in all publications are solely those of the individual author(s) and contributor(s) and not of MDPI and/or the editor(s). MDPI and/or the editor(s) disclaim responsibility for any injury to people or property resulting from any ideas, methods, instructions or products referred to in the content.